Energy Proceedings
Vol 52, 2025
ISSN 2004-2965

A Physics-based Data-driven Simulation Method Coupling the Time-varying Properties and High-speed non-Darcy Flow under Waterflooding#

Boying Li[1], Xinwei Liao[1*], Lingfeng Zhang[1], Dongzhi Yan[2], Zhonghao Li[3]

1 State Key Laboratory of Petroleum Resources and Prospecting, China University of Petroleum (Beijing)

2 CNOOC Energy Development Equipment Technology Co., Ltd

3 Oil Production Technology Institute, PetroChina Da-gang Oilfield Company
(Corresponding Author: Xinwei Liao, Email: 2022310159@student.cup.edu.cn)

ABSTRACT

For long-term waterflooding reservoirs with strong heterogeneousness, the high-intensity water flooding has caused significant time-variation in reservoir properties; Meanwhile, there are varying degrees of high-speed non-Darcy flow features in the thief zone. In this paper, a new physical-based dimensionality reduction numerical simulation method is proposed, which takes the one-dimensional connection flow units as the research object, with the dynamic transmissibility and pore volume as the characteristic parameters. By coupling the time-varying properties and high-speed non-Darcy flow, a fine simulation of strongly heterogeneous reservoirs considering the thief zone in long-term waterflooding has been realized. We analyze the effects of time-varying physical properties and high-speed non-Darcy flow on the dynamics of long-term waterflooding taking the channelized Egg model as an example. The results show that by the high-intensity water flooding, the physical properties and conductivity of the thief zone become better, which accelerates the waterflood front broken, the water cut rises, and the residual oil between the wells is enriched; On the opposite side of the small pore throat. Influenced by the non-Darcy flow in the thief zone, the conductivity and fluid seepage capacity in the thief zone decreases, and the inhibition of the water is more significant, and more water flows to the small pore throat, which enlarges the swept volume, and facilitates the recovery. Based on the method proposed in this article, a more precise and efficient simulation of heterogeneous waterflooding reservoirs has been achieved.

Keywords: dimensionality reduction simulation, long-term waterflooding, high-speed non-Darcy flow, physical properties time variation, inter-well connectivity

NONMENCLATURE

∇P_l	Pressure Gradient, MPa/m
μ_l	fluid viscosity, mPa·s.
$\overline{\rho_l}$	fluid density, kg/m^3
dt	time step, s
v	seepage rate, cm/s
$C_{t,j}$	total compressibility, MPa^{-1}
$V_{i,t}$	The control volume of node i, m^3
S_{wp}	Water saturation at x_p
f'_w	Derivative of water cut
m	A vector of feature parameters
φ	Porosity of rocks
k_{rl}	Relative permeability of oil and water
β	High-speed non-Darcy coefficient, m^{-1}
L_{ij}	Distance between two nodes i and j, m
E_d	dynamic covariance matrix
N_t	Multiples of change in permeability
k	Permeability, md
T_t, T_{in}	Transmissibility before and after time-varying, m^3·d^{-1}·MPa^{-1}
K_t, K_{in}	Permeability before and after time-varying, m^3·d^{-1}·MPa^{-1}
Q_i	Source-sink phase of node i, m^3/s
A_{ij}	Area between control *body* i and j, m^2
$Q(t)$	Cumulative flow volume at time t, m^3
P_V	displacement multiple, m^3/m^3
x_p	Upstream position at node x
R	Objective function for history matchting
$S(m)$	Vector of model predicted dynamic indicators
$T_{i,j}$	Transmissibility between nodes i and j, m^3·d^{-1}·MPa^{-1}
G_{ij}	Mass flow of control body j flowing into i through A_{ij}
q_l	the source-sink phases of injectors and productor, m^3/s

This is a paper for the 16th International Conference on Applied Energy (ICAE2024), Sep. 1-5, 2024, Niigata, Japan.

p_i, p_j	Average pressure at nodes *i* and *j* , MPa
E_V	displacement flux, m^3/m^2
d_{obs}	Vector of dynamic indicators of observations

1. INTRODUCTION

A large number of mine and experimental data show that: in the long-term waterflooding, the reservoir physical properties of significant changes [1], [2], [3], and part of the thief zone no longer meet the linear Darcy seepage features. The Forchheimer and the exponential equation can be used for the description of high-speed nonlinear flows. the Forchheimer equation [4] can be derived from the N-S equation with a clear theoretical basis. The exponential equation is simple to calculate but lacks theoretical guidance [5]. However, most of the researches are limited to the study of nonlinear flow of gases in porous media [6],[7], while there are fewer studies on oil and water. Meanwhile, most of the numerical simulation on the time-varying of reservoir properties under waterflooding have only examined a single time-varying law [8],[9], while reservoirs with different characteristics have different time-varying laws.

Traditional numerical simulation methods rely on large-scale geologic parameters and fine grids, which are computationally too expensive. Therefore, surrogate models based on physical dimensionality reduction and data-driven models have become favorable substitutes. However, data-driven surrogate models require a large number of high-fidelity numerical simulation results and do not have a clear physical basis [10],[11], and the process is basically limited to the mechanism model, which makes it difficult to realize the surrogate for large-scale reservoirs. In contrast, the physical-data dual-driven numerical simulation model [12],[13], which has a clear physical meaning, has a significant advantage in computational efficiency and accuracy in the surrogate process of large-scale numerical simulation, and accelerates the closed-loop reservoir management process. However, this method does not fully consider the complex mechanism under waterflooding.

Therefore, this method based on dual physical-data drive is further extended in this work. The time-varying of physical properties are described by the characterization of inter-well displacement flux and dynamic conductivity; and the characteristics of high-speed non-Darcy flow in thief zones are considered by the Forchheimer equation. By coupling the two mechanisms, a finer and more efficient simulation of strongly heterogeneous waterflooding reservoirs is realized, and the effects of time-varying reservoir properties and high-speed non-Darcy flow on the development performance are clarified.

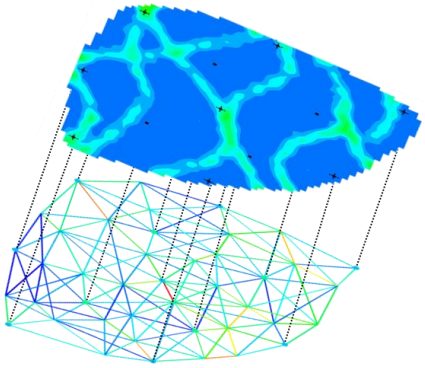

Fig. 1 Physics-based dimensionality reduction model

2. METHODOLOGY

2.1 Mechanism of high-speed non-Darcy flow

Consider discretizing the three-dimensional reservoir into a two-dimensional model consisting of a series of one-dimensional connective units. Based on Forchhmer law, the nonlinear flow in the thief zone and the Darcy flow in the small pore throat are considered; The high-speed non-Darcy flow coefficient β is introduced. In the small pore throat, β=0; in the thief zone, β >0, and the velocity satisfies the quadratic nonlinear relationship with the pressure gradient:

$$-\nabla P_l = -\left(\frac{\mu_l}{kk_{rl}} v_l + \beta \overline{\rho} v_l^{\,2}\right) \tag{1}$$

Then the continuous equation of fluid flow in the thief zone can be expressed as:

$$-\nabla \cdot (\overline{\rho_l} v_l) + q_l = \frac{\partial}{\partial t}\left(\phi \overline{\rho}\right) \tag{2}$$

By combining equations (1) and (2):

$$-\frac{\partial p}{\partial x} = \frac{\mu}{kk_{rl}\delta} v_l, where, \delta = \left(1 + \frac{kk_{rl}}{\mu}\beta \overline{\rho} v_l\right)^{-1} \tag{3}$$

Consider integrating equation (2) over the time step Δt and control volume *V*:

$$\begin{aligned} &\iint_{dtV} \nabla \cdot (\overline{\rho_l} v_l) dV dt + \iint_{dtV} q_l dV dt \\ &= \int_{dt} \frac{\partial}{\partial t}\left(\int_V \phi \overline{\rho_l} dV\right) dt \end{aligned} \tag{4}$$

Consider an approximation of Eq. (4) using the sum of normal vectors between neighboring grids that meets the physical meaning, based on time integration followed by estimation using the rectangular method:

$$\sum_{j=1}^{n} G_{ij} + Q_i = C_{t,i}(\mathrm{p}_i^{t+\triangle t} - \mathrm{p}_i^{t})\frac{V_t}{\triangle t}$$
$$G_{ij} = A_{ij}\frac{kk_{rl}\delta}{\mu L_{ij}}\nabla p, T_{ij} = A_{ij}\frac{kk_{rl}\delta}{\mu L_{ij}} \quad (5)$$

2.2 Mechanism of high-speed non-Darcy flow

Based on Buckley-Leverett theory [15], the water saturation and cumulative flow volume at any location from the injection satisfy the equation (6):

$$\frac{dx}{dt} = \frac{Q(t)}{\phi A}\frac{df_w}{dS_w} \quad (6)$$

In order to eliminate the influence of well spacing on the displacement multiple and to enhance the rationality and stability, define the displacement flux:

$$E_V = P_V(x_p - x) = \frac{\int_{t=0}^{t=T} Q_t f_w dt}{A\phi} \quad (7)$$

The time-varying characterization model for permeability (transmissibility) is obtained by regression based on long-term waterflooding experiments:

$$N_t = K_t / K_{ini} = T / T_{ini} = F(E_V) \quad (8)$$

2.3 Solving the coupled material balance equation

The material balance equation coupling the high-speed non-Darcy flow with the time-varying permeability can be obtained by bringing Eq. (8) into Eq. (5):

$$\sum_{j=1}^{n}\sum_{l=o,w} A_{ij}\frac{k(E_V)k_{ri}\delta(E_V)}{\mu_l L_{ij}}(p_i - p_j) + Q_i$$
$$= \frac{C_{t,i}(p_i^{t+\triangle t} - p_i^{t})V_{ti}}{\triangle t}, where, Q_i = \sum_{l=o,w}\frac{q_l V_i}{\rho} \quad (9)$$

2.4 Inversion of characteristic parameters

The history matching objective function is established based on Bayesian theory. By matching the dynamic indicators such as oil production rate and water cut, the inversion obtains the conductivity and control volume in accordance with the actual geological characteristics.

$$\min R(m) = \frac{1}{2}\left[s(m) - d_{\mathrm{obs}}\right]^{\mathrm{T}} E_{\mathrm{d}}^{-1}\left[s(m) - d_{\mathrm{obs}}\right] \quad (10)$$

3. METHODOLOGY

3.1 model verification

Based on the Egg model [14], a numerical simulation model considering channelized thief zone was established. The total number of meshes of the model: 60 × 60 × 7, and the number of active meshes is 18553. The specific parameters are shown in Table 1:

As shown in Fig. (2) are the permeability, porosity, inverted transmissibility and pore volume models respectively; The transmissibility distribution can well describe the thief zone.

Table 1 Parameters of the model

Parameter	Value
Mesh Size	4m×4m×8m
Porosity	0.20
Water compression coefficient	1.0×10^{-5}Mpa^{-1}
Oil compression coefficient	1.0×10^{-5}Mpa^{-1}
Initial formation pressure	39.5MPa
Viscosity of water	1mPa·s
Viscosity of oil	5mPa·s
Initial water saturation	0.2

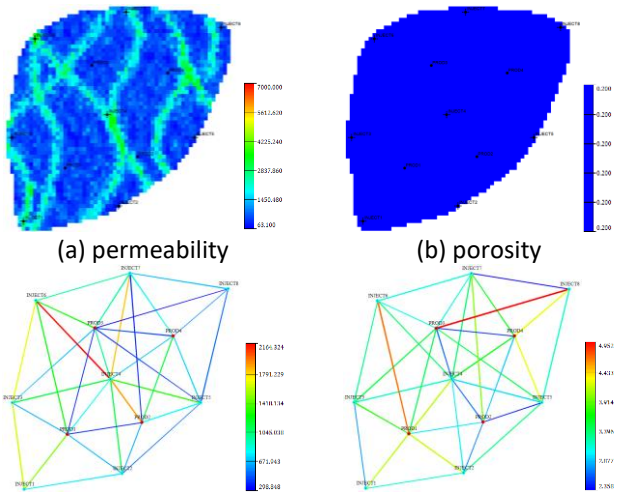

(a) permeability (b) porosity

(c) inversed transmissibility (d) inversed pore volume

Fig. 2 Distribution of property fields

The results of the *tNavigator* are taken as the observed value, the time-varying and non-Darcy flow mechanisms are not considered. As shown in Fig. 3 are the matching results of oil production rate and water cut. The average matching accuracy of oil production rate and water cut are 95.28% and 94.43%, respectively; the calculation time of this paper's method and *tNavigator* are 1.38s and 28s, respectively. The accuracy and high efficiency of this paper's model are verified.

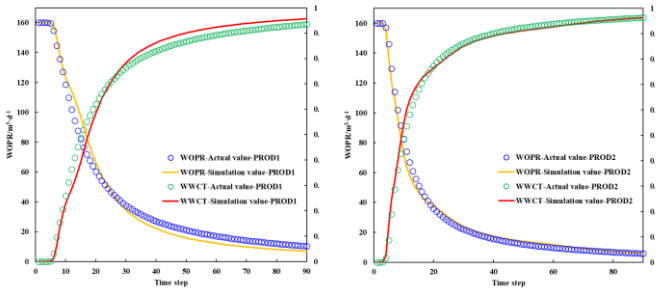

(a) PROD1 (b) PROD2

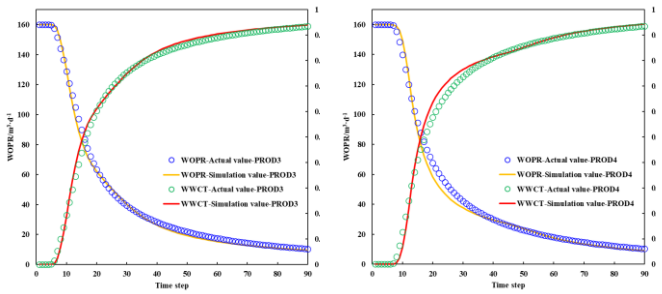

(c) PROD3 (d) PROD4

Fig. 3 Results of history matching

3.2 Results analysis

To further clarify the impact of time-varying reservoir properties and non-Darcy flow in the thief zone on dynamics, consider:

(1) Influenced by the waterflooding, when K_{ij}<=2 μm^2, particle sedimentation and bridge plugging dominate, and the inter-well transmissibility decreases with the increasing of the displacement flux; When 2 μm^2 <K_{ij}< 4 μm^2, particle sedimentation, bridge plugging, and migration are all present, and the Inter-well transmissibility first decreases and then increases with increasing displacement fluxes; When K_{ij} >=4 μm^2, particle migration within the thief zone dominates, and the inter-well transmissibility increases with the increasing of the displacement flux. The specific model is shown in equation (11)-(13):

$$\begin{aligned} &low\ permeability: T_{ini} < 500 \\ &N_t = 0.064LN(E_V) + 0.8 \end{aligned} \tag{11}$$

$$\begin{aligned} &medium\ permeability: 500 \le T_{ini} \le 1500 \\ &N_t = 0.43LN(E_V) - 0.31 \end{aligned} \tag{12}$$

$$\begin{aligned} &high\ permeability: T_{ini} > 1500 \\ &N_t = 0.75LN(E_V) - 1.26 \end{aligned} \tag{13}$$

(2) When K_{ij} <=4μm^2, the fluids seepage pattern between wells is considered as Darcy flow; when K_{ij} >4μm^2, which is high-speed non-Darcy flow. And based on the empirical formula [5], it is determined that β≈8.5×10^5.

3.2.1 Web references

The dynamics of transmissibility for PROD1-INIECT1, PROD2-INIECT7, PROD3-INIECT4, and PROD4-INIECT8 considering different mechanisms are shown in Fig. 4.

(1) Between PROD1 and INIECT1 is controlled by the thief zone together, which are dominated by particle migration under the effect of long-term waterflooding, and the physical properties of the reservoir become better, and the transmissibility increases; when the high-speed non-Darcy flow in the thief zone is taken into account, the pressure gradient in the process of seepage is determined by viscous and inertial forces together, and the transmissibility decreases; when the effects of both are taken into account comprehensively, the transmissibility firstly decreases and then increases. The increase reaches 92.17%.

(2) Between PROD2 and INIECT7 is controlled by the thief zone and small pore throat together, the connectivity is poor, the effect is dominated by particle sedimentation and bridge plugging, and the physical properties of the reservoir are deteriorated; the fluid between the wells is Darcy flow; when the effects of the two are taken into account together, the transmissibility decreases, and the decrease is up to 46.49%.

(3) Between PROD3 and INIECT4, it is controlled by the thief zone and small pore throat together; Considering that particle sedimentation, bridge plugging, and migration are all present under the effect of long-term waterflooding, reservoir physical properties get worse and then better; some degree of non-Darcy flow exists between wells; When considering the effects of the two, the transmissibility decreases first and then increases, with an increase of 67.34%.

(4) Between PROD4 and INIECT8 is controlled by thief zone and small pore throat together; considering the particle sedimentation, bridge plugging, and migration are all present under the effect of long-term waterflooding, the physical properties of the reservoir deteriorate firstly and then improve; some degree of non-Darcy flow exists between wells; when the effects of the two are taken into account together, the transmissibility decreases firstly and then increases, with the increase amounting to 80.81%.

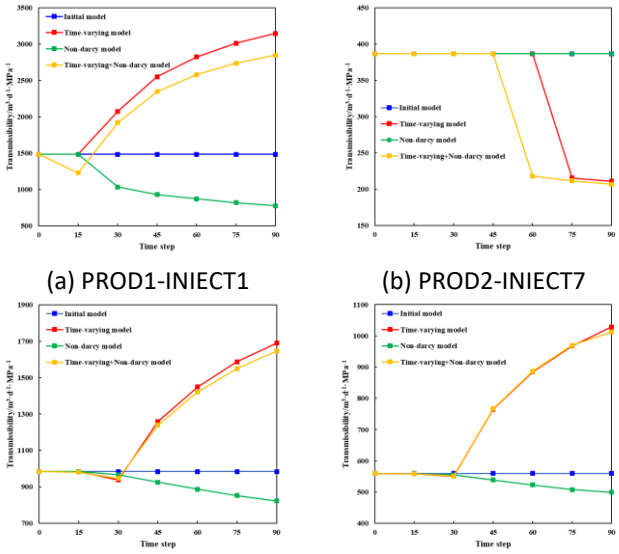

(a) PROD1-INIECT1 (b) PROD2-INIECT7

(c) PROD3-INIECT4 (d) PROD4-INIECT8

Fig. 4 Dynamics of transmissibility

3.2.2 *Dynamics of water cut*

The dynamics of water cut for PROD1-INIECT1, PROD2-INIECT7, PROD3-INIECT4, and PROD4-INIECT8 considering different mechanisms are shown in Fig. 5.

(1) Compared with the initial model, PROD1 is affected by particle sedimentation, bridge plugging and migration, and Darcy, non-Darcy flow effects together. And it is most significantly affected by INIECT1.

(2) Compared with the initial model, PROD2 is mainly affected by the particle migration and non-Darcy flow. particle migration accelerates the waterflood front broken, while non-Darcy flow inhibits fluid flow and has a more pronounced effect on the water.

(3) Compared with the initial model, PROD3 is affected by particle sedimentation, bridge plugging and migration, and Darcy and non-Darcy flow effects together.

(4) Compared with the initial model, PROD4 is affected by particle sedimentation, bridge plugging and migration, and Darcy flow. The water cut decreases firstly and then increases.

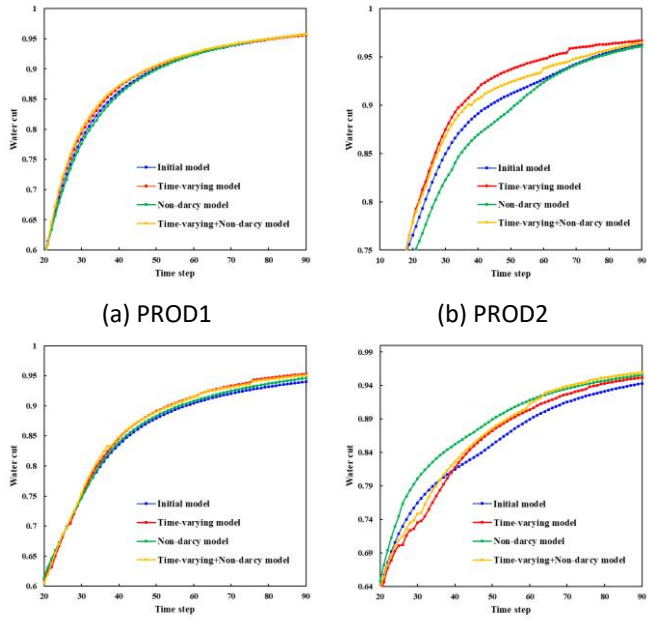

(a) PROD1 (b) PROD2

(c) PROD3 (d) PROD4

Fig. 5 Dynamics of water cut

3.2.3 *Dynamics of residual oil*

As shown in Fig. 6, when considering the effect of time-varying reservoir properties, the properties of thief zone become better, the injected water breaks through quickly along the preferential path, and a large amount of residual oil is enriched; The properties of small pore throat become worse, and the waterflood sweep efficiency increases, and part of the residual oil is recovered; when considering the existence of non-Darcy flow in l thief zone, it inhibits the flow, and the inhibition of the water phase is more powerful. Under the fixed production system, it is conducive to the extraction of oil.

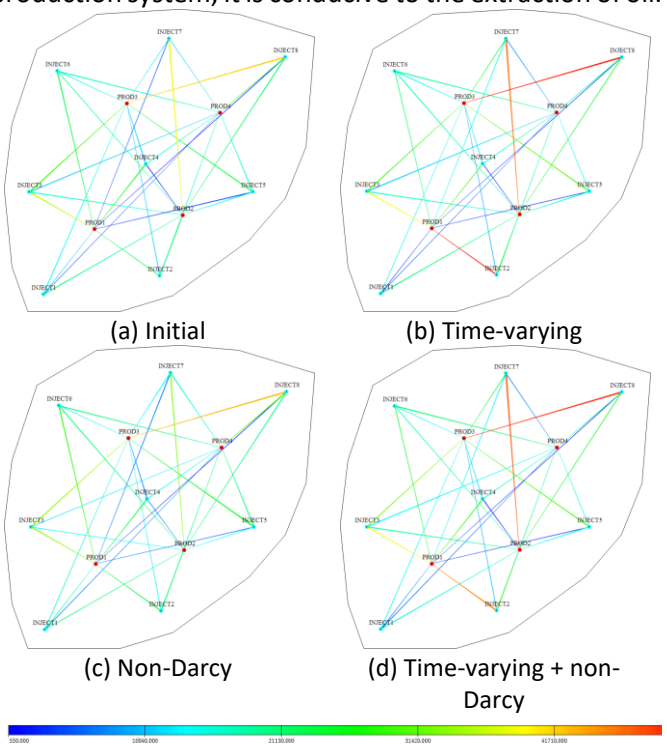

(a) Initial (b) Time-varying

(c) Non-Darcy (d) Time-varying + non-Darcy

Fig. 6 Dynamics of residual oil

4. Discussion and conclusions

(1) In this paper, a coupled model considering different reservoir time-varying and high-speed non-Darcy flow characteristics during long-term waterflooding is established by extending the reduced-dimensional numerical simulation method based on physical-data dual-drive.

(2) When different reservoir time-varying characteristics are considered, the seepage capacity of thief zone is enhanced, which accelerates the waterflood front broken. The residual oil between wells is enriched; the opposite is true in small pore throat.

(3) When considering the characteristics of high-speed non-Darcy flow in thief zone, the pressure gradient in thief zone is caused by viscous and inertia together, the seepage capacity decreases, and the inhibition of water is more significant, more water flows to the small pore throat, and the residual oil between wells decreases, which is conducive to balanced exploitation.

(4) When coupling the two mechanisms is considered, the physical time-varying effects have a more significant impact on development.

ACKNOWLEDGEMENT

Xinwei Liao would like to express his gratitude to the China Important National Science & Technology Specific

Projects (Grant No. 2017ZX05009004-005), the National Natural Science Foundation of China (Grant No. 52074322, U1762210) for their generous financial support of the research.

REFERENCE

[1] H. Jia, R. Zhang, X. Luo, Z Zhou and L. Yang. Nuclear magnetic resonance experiments on the time-varying law of oil viscosity and wettability in high-multiple waterflooding sandstone cores[J]. Petroleum Exploration and Development,2024,51(02):394-402.

[2] Q. Du. Variation law and microscopic mechanism of permeability in sandstone reservoir during long term water flooding development[J]. Acta Petrolei Sinica, 2016,37(09):1159-1164.

[3] R. Cao, Z. Dai, Z. Wang, Y. Wang, J. Jiang, H. Li and Z. Jia. Displacement behavior and mechanism of long-term water flooding in sandstone oil reservoirs[J]. Journal of Central South University,2021,28(3):834-847.

[4] W. Liu and J. Cui. A Two-Grid Block-Centered Finite Difference Algorithm for Nonlinear Compressible Darcy–Forchheimer Model in Porous Media[J]. Journal of Scientific Computing,2018,74(3):1786-1815.

[5] Y. Yao, G. Li and P. Qin. Seepage features of high-velocity non-Darcy flow in highly productive reservoirs[J]. Journal of Natural Gas Science and Engineering, 2015,271732-1738.

[6] Y. Wang, B. Wang, J. Luo, C. Zhao and L. Shi. Investigation of Dominant Factors Influencing High-speed Non-Darcy Effect in Gas Wells[J]. Journal of Southwest Petroleum University (Science & Technology Edition),2024,46(02):87-94.

[7] K. Shang, D. Feng, L. Ye and H. Liu. Analysis of the Influence of the Development of Fracture-porosity-type Volcanic Gas Reservoir[J]. Journal of Southwest Petroleum University (Science & Technology Edition), 2018,40(02):107-114.

[8] J. Rui, X. Qiao, W. Teng, J. Xu and Z. Sun. Impact of physical properties time variation on waterflooding reservoir development[J]. Fault-Block Oil & Gas Field, 2016,23(06):768-771.

[9] P. Zhao, Z. Shen, M. Cai, J. Zhang and R. Jiang. A comprehensive reservoir simulation technique based on time-varying petro-physical parameters characterized by effective displacement flux[J]. Journal of China University of Petroleum (Edition of Natural Science), 2022,46(01):89-96.

[10] S. Wang, J. Xiang, X. Wang, Q. Feng, Y. Yang, X. Cao and L. Hou. A deep learning based surrogate model for reservoir dynamic performance prediction[J]. Geoenergy Science and Engineering,2024,233212516-.

[11] Z. Feng; Z. Tariq, X. Shen, B. Yan, X. Tang and F. Zhang. An encoder-decoder ConvLSTM surrogate model for simulating geological CO_2 sequestration with dynamic well controls[J]. Gas Science and Engineering, 2024,125205314-.

[12] W. Liu, H. Zhao, G. Sheng L. Xu and Y. Zhou. A rapid waterflooding optimization method based on INSIM- FPT data-driven model and its application to three-dimensional reservoirs[J]. Fuel,2021;292:120219.

[13] Z. Guo and A C. Reynolds. INSIM-FT in three-dimensions with gravity[J]. Journal of Computational Physics,2018,380143-169.

[14] JD. Jansen, RM. Fonseca, S. Kahrobaei, MM. Siraj, GMV. Essen and PMJVD. Hof. The egg model-a geological ensemble for reservoir simulation[J]. Geoscience Data Journa,2014,1(2):192-195.

[15] H. Zhao, L. Xu, Z. Guo. Q. Zhang, W. Liu and X. Kang. Flow-Path Tracking Strategy in a Data-Driven Interwell Numerical Simulation Model for Waterflooding History Matching and Performance Prediction with Infill Wells[J]. SPE JOURNAL,2020,25(2):1007-1025.